metals

MDPI

Article

Analysis of Stored Energy Distribution in Three Directions of Tantalum in Deformed and Annealed States

Yanjun Zhou [1,2,*], Yahui Liu [3,*], Qianqian Zhu [1] and Shaodan Yang [4,5]

[1] School of Materials Science and Engineering, Henan University of Science and Technology, Luoyang 471023, China; zhuqianqian@haust.edu.cn
[2] Henan Key Laboratory of Advanced Conductor Materials, Zhengzhou 450046, China
[3] School of Mechatronics Engineering, Henan University of Science and Technology, Luoyang 471023, China
[4] School of Material Science & Engineering, Zhengzhou University, Zhengzhou 450001, China; sdyang@hnas.ac.cn
[5] Institute of Materials, Henan Academy of Sciences, Zhengzhou 450046, China
* Correspondence: zhouyanjun@haust.edu.cn (Y.Z.); liuyh75@haust.edu.cn (Y.L.); Tel.: +86-13937955371 (Y.Z.); +86-19942238232 (Y.L.)

Abstract: Microstructures in high-purity tantalum (Ta) were analyzed in three directions, focusing on the evolution of stored energy during rolling and heating processes. Results indicated significant fluctuation in the transaction direction (TD) surface, which was observed in both deformed and annealed states. This phenomenon is attributed to the alternately arranged {111}<uvw>(<111>//normal direction (ND)) and {100}<uvw>(<100>//ND) oriented grains, coupled with the substantial energy difference between them, even after 12 passes. Additionally, through the estimation and calculation of stored energy based on band contrast from electron backscatter diffraction and X-ray line profile analyses, the recovery kinetics for different directions and grain types were quantitatively assessed. Findings revealed that the dislocation density of {111} grains decreased significantly more than that of {100} grains when annealed at 1073 K. The degree of recovery was closely related to temperature, dislocation density, and dislocation type.

Keywords: tantalum; stored energy; electron backscattering diffraction; dislocation; recovery

Citation: Zhou, Y.; Liu, Y.; Zhu, Q.; Yang, S. Analysis of Stored Energy Distribution in Three Directions of Tantalum in Deformed and Annealed States. *Metals* **2024**, *14*, 1298. https://doi.org/10.3390/met14111298

Academic Editor: Andrea Di Schino

Received: 22 September 2024
Revised: 4 November 2024
Accepted: 14 November 2024
Published: 17 November 2024

1. Introduction

Tantalum (Ta) is a type of transition metal with a high density (16.69 g/cm^3) and a high melting point (3269 K), and is widely used in many fields, including electrical capacitor manufacture, superalloys, chemical processing, sputtering targets, etc. [1]. The sputtering rate highly depends on the crystallographic orientation of each grain due to the different densities of clustering atoms at different crystallographic planes. Thus, sputtering performance and coating quality depend on microstructure homogeneity [2–4]. Microstructural homogeneity, which specifically means the distribution of grain size, grain aspect ratio, and grain orientations, is greatly influenced by the recrystallization process, which mainly includes the nucleation and growth of grains during the annealing process. And the nucleation and growth of grains are closely related to the distribution of stored energy, which refers to various dislocations formed during the plastic deformation of metals [5–7].

Rolling is a common fabricating technology that is mainly used to process metal sheets [8,9]. Unidirectional rolling always leads to strong strain concentration in the local region upon deformation. Next, it leads to the formation of microbands or even microbands in grains, leading to inhomogeneous deformation [10]. However, a 135° clock rolling change in the strain path, in which the sample is clock rotated by 135° around the ND of the sample between consecutive rolling paths, can effectively homogenize deformed structures and the distribution of stored energy in Ta sheets [11]. In previous studies, the

influence of the strain path on the evolution of texture and dislocation structures during rolling was investigated in detail [10]. However, these investigations were limited to a specific direction of the sheet, and stored energy was not discussed in detail in terms of anisotropic aspects or microstructural development during the annealing process. These are essential for understanding the fundamental deformation mechanism of clock rolling and the microstructural control of Ta sputtering targets. The microstructural state of the target material in different directions, especially the consistency or uniformity of deformation, directly affects the deposition state of tantalum atoms during the subsequent magnetron sputtering process and the stability of chip products during service. Understanding the evolution of microstructural states in different directions during the rolling process is essential for the design and optimization of subsequent deformation and heat treatment processes. Such studies are relatively scarce in the literature.

The results of electron backscattering diffraction (EBSD), X-ray line profile analysis (XLPA), and Vickers hardness test experiments of clock-rolled and recovered Ta samples are presented herein. Systematic stored energy distribution studies of deformed and annealed samples are demonstrated in three directions (RD, ND, and TD). An attempt was made to establish a link between rolling direction and deformed microstructure in different directions of the sample in order to design an optimized rolling process for future industrial production.

2. Materials and Methods

The Ta (99.95 wt.%) sheet was annealed at 1523 K for 2 h in a vacuum environment to obtain a fully recrystallized microstructure. The chemical composition is shown in Table 1, and rolling parameters are listed elsewhere [12]. Next, the sheet, with a thickness of 20 mm and an average grain size of 50 μm, was 135° clock rolled to an 82% reduction in thickness (12 rolling paths in total). Two samples ($10^{L} \times 8^{W} \times 3.6^{T}$ mm^3) were cut from the as-rolled Ta sheet. The subsequent annealing procedure was executed in a vacuum atmosphere at 1073 K for 60 min to obtain a recovery state.

Table 1. The chemical composition of Ta (ppm wt.%).

C	N	H	O	Nb	Mo	W	Ti	Si	Fe	Ni	Ta
9	20	2	30	6.4	0.14	0.61	<0.001	<0.005	<0.005	<0.005	Balance

EBSD observation was focused on all three surfaces (TD, ND, and RD surfaces) of deformed and annealed samples. Blue boxes show testing positions in Figure 1. It should be noted that the microstructure of the ND surface was characterized after the sliver of sample along the central layer of the ND surface. As shown in Figure 1, the sample was sliced along the red line, and the ND surface of the sliced sample was characterized to ensure that ND data were more representative. Testing surfaces were prepared by mechanical grinding and polishing, followed by electrolytic polishing with a mixture of hydrofluoric acid and sulfuric acid (1:9 by volume) at 298 K. EBSD measurements were conducted on a JEOL-JSM-7800F scanning electron microscope (JEOL Ltd., Tokyo, Japan) with an accelerating voltage of 20 kV. Data acquisition and analysis were processed on an Aztec system (Oxford instruments, Abingdon, United Kingdom) and the Channel 5 software (Oxford instruments, Abingdon, United Kingdom) equipped in this system, respectively.

The X-ray line profile for the central layer along the ND surface (green box in Figure 1) was measured by an X-ray diffractometer (XRD, Rigaku D/max 2500 PC) (Rigaku, Japan) with Cu Kα radiation. The (200) and (222) line profiles, the second-order diffractions of {100} and {111} orientations, respectively, were recorded in the step-scan mode and then fitted by JADE 6.5 software to calculate the stored energy of the {100}− and {111}−oriented grains. Herein, {100} and {111} are used to represent {100}<uvw>(<100>//ND) and {111}<uvw>(<111>//ND), respectively.

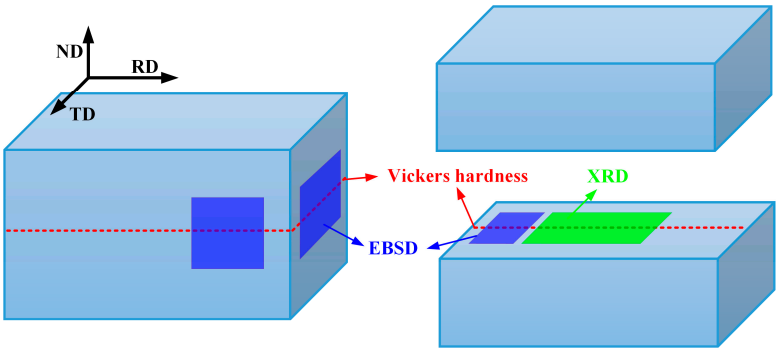

Figure 1. Testing positions for EBSD, XRD, and Vickers hardness measurements in the sample. The same positions were cut along the central layer of the RD surface. Red dashed lines indicate the sample's midplane.

Vickers hardness (HV) measurements were carried out on an MH-5 L model hardness tester (Everone, Shanghai, China) with a load of 500 g and a dwell time of 10 s. Testing surface preparation was the same as that for EBSD. Thirty in line measurements were made for every surface in the three directions, as shown by red lines in Figure 1.

3. Results

3.1. Deformation Microstructure

Figure 2 is a 3D reconstructed orientation imaging map (OIM) of the three surface directions of the deformed sample. The microstructures in these three surfaces showed significant differences after clock rolling. The initial grains evolved into 'pancake' shapes on the ND surface, and grains stretched to some extent along the RD direction. For RD and TD surfaces, the initial grains evolved into banded shapes, and grain boundaries showed a certain degree of bending and fluctuation along the TD and RD directions, respectively. Many grains in the TD and RD surfaces split during deformation, and grain boundaries of adjacent grains infiltrated and intertwined with each other. Distances between neighboring grains were not the same on TD and RD surfaces, and the distance was shorter on the TD surface than it was on the RD surface; namely, grains were more severely split on the TD surface. The rolling texture of all three surfaces was mainly composed of {111} and {100} orientations, as shown in blue and red, respectively.

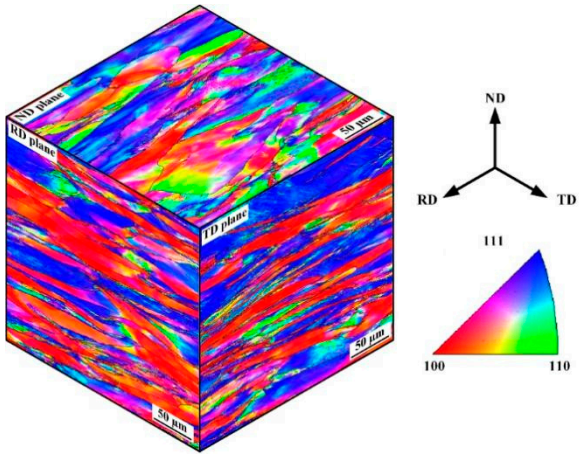

Figure 2. Reconstructed orientation imaging maps (OIMs) of surfaces in three directions of 135° clock-rolled sample.

3.2. Annealed Microstructure

After annealing at 1073 K for 60 min, as shown in Figure 3, microstructural observation revealed initial deformed grains elongated in the RD direction and banded (as indicated by the yellow arrow) in the TD and RD directions, without any signs of recrystallization. As reported in previous studies, the deformed Ta sheet mainly showed recovery behaviors at 1073 K [13]. In this period, the rearrangement of dislocations appeared, and some cell structures formed in local regions.

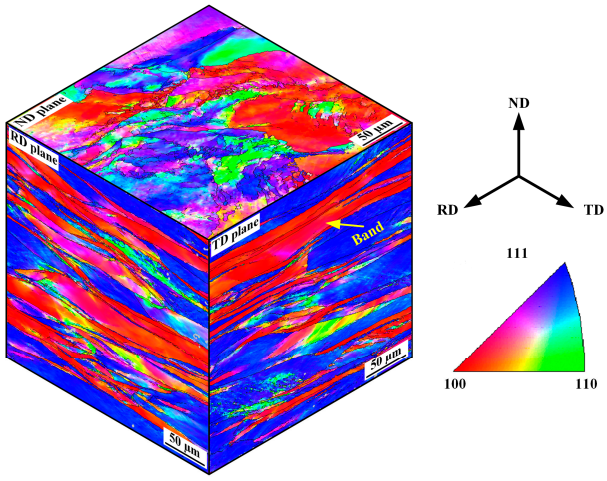

Figure 3. Reconstructed orientation imaging maps (OIMs) of surfaces in three directions of annealed sample.

3.3. Vickers Hardness Measurement

In addition, the deformation and annealed hardness of different test surfaces were tested, as shown in Figure 4a, which shows the hardness value distribution for the deformation state. The average hardness values for TD, RD, and ND surfaces were 153.31 ± 5.81, 151.32 ± 6.64, and 148.97 ± 10.26, respectively, with both TD and RD surfaces exhibiting higher hardness than the ND surface. However, as shown in Figure 4a, the ND surface showed significantly greater fluctuation in hardness values.

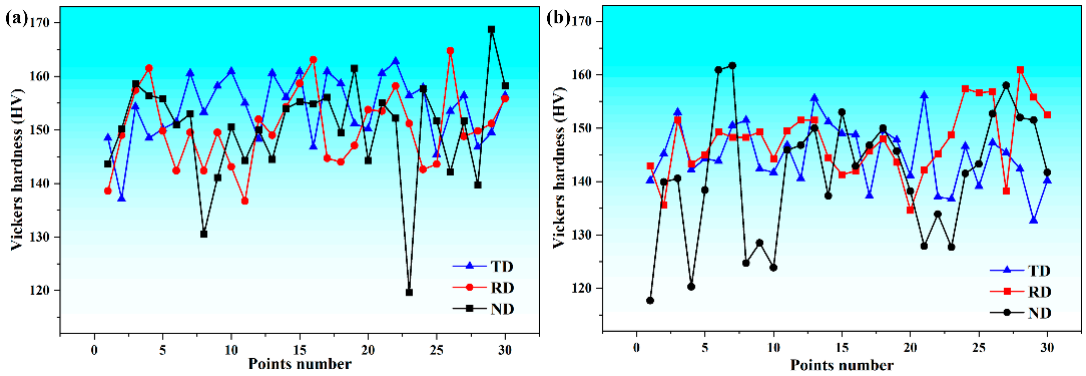

Figure 4. Vickers hardness values for different planes in deformed and annealed states: (**a**) deformed state and (**b**) annealed state.

After annealing, the hardness of different surfaces were tested again. It was found that hardness values all decreased, but these decreases were not significant, as shown in Figure 4b. Among them, the average values of the three surfaces were 145.06 ± 5.6, 146.29 ± 6.23, and 140.01 ± 11.01, respectively. Similarly, the degree of value fluctuation for different surfaces did not change significantly.

4. Discussions

The results from EBSD demonstrate the deformed and annealed microstructure of Ta, as shown in Figures 2 and 3, and there seems to be no obvious difference between them. Most of the energy expended in rolling metal is emitted as heat, and only a small amount (~1%) remains as energy stored in the material. Generally, stored energy is mainly derived from accumulated dislocations generated during rolling, and the essential difference between deformed and annealed states lies in the dislocation content and arrangement [14–17]. From this point of view, the difference is mainly based on the density, distribution, and morphology of dislocations [16,18].

4.1. XLPA for Stored Energy

Rolling deformation leads to changes in lattice spacing and distortions. Lattice distortions then lead to the broadening of X-ray diffraction peaks, which can be employed to calculate the stored energy [19,20]. As {111} and {100} orientations are the primary orientation types in both as-rolled and annealed samples, this paper focuses on them in the following discussions.

Figure 5 shows fitted X-ray line profiles for (200) and (222) diffraction peaks, which were formed from the second-order diffraction of {100} and {111} orientations, respectively. The effective broadening (B) can be estimated from the following equation [19]:

$$B^2 = B_r^2 - B_a^2 \quad (1)$$

B_r and B_a are the measured values of the full width at half maximum (FWHM) of deformed and fully recrystallized samples. Next, the lattice strain ($\Delta d/d$), which leads to broadening, can be calculated based on the following equation [19]:

$$\frac{\Delta d}{d} = \frac{B}{2\tan\theta} \quad (2)$$

in which θ is the Bragg angle. And the stored energy, E_i, for orientation "i", can be calculated according to the Stibitz formula [19]:

$$E_i = \frac{3}{2} Y_{hkl} \frac{(\Delta d/d)^2}{(1 + 2v_{hkl}^2)} \quad (3)$$

in which Y_{hkl} and v_{hkl} are the Young's Modulus and Poisson's ratio, respectively. They were 387.93 GPa and 0.36 for {111} orientations, respectively, and 197.3 Gpa and 0.38 for {100} orientations, respectively [21,22]. Next, the stored energies for differently oriented grains were calculated, as listed in Table 2. The stored energy of {111} orientations in the deformed state was larger than that of {100} orientations, which is in accordance with previous investigations [10]. After annealing at 1073 K for 60 min, the stored energy for both {111} and {100} orientations reduced; {111} orientations experienced a significant decrease of about 64%.

This large amount of stored energy reduction in {111} grains was mainly due to the change in dislocation morphology upon recovery. Dislocations exist in tangled dislocations, high-density dislocation walls, or cells in {111} grains. The dislocation density was larger than that of {100} grains, most of which had low-angle boundaries. This kind of dislocation is easily rearranged and annihilated, and evolves into multiple kinds of substructures, like big cells or subgrains, leading to a significant reduction in dislocation density during heating. Although the distribution of dislocations in {100} grains is relatively homogeneous, this dislocation is not prone to be annihilated or merged into larger cells or subgrains during annealing [23]. In other words, this is one of the reasons why {100} grains always have a low nucleation rate and recrystallization kinetic in tantalum and other common body-centered cubic (BCC) metals upon annealing.

It should be noted that the calculation of stored energy based on XLPA provides an insight declaration of stored energy change before and after annealing treatment at a macro scale. However, the distribution of stored energy in some local regions, such as different surfaces in a sample, cannot be analyzed in detail using XLPA.

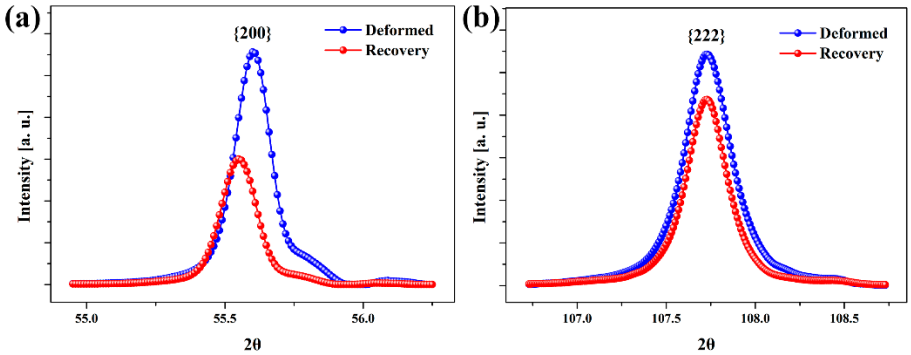

Figure 5. Fitted (200) and (222) diffraction peaks of deformed and annealed specimens, respectively: (**a**) (200) peak and (**b**) (222) peak.

Table 2. Orientation-dependent stored energies and relevant parameters used for stored energy calculation.

	θ_{200}	θ_{222}	B_{r200}	B_{r222}	$B_{\alpha 200}$	$B_{\alpha 222}$	E_{200}	E_{222}
Deformed	55.60°	107.74°	0.16°	0.32°	0.13°	0.16°	1.35 J/mol	4.92 J/mol
Annealed	55.56°	107.73°	0.15°	0.29°	0.13°	0.16°	0.69 J/mol	1.75 J/mol

4.2. Band Contrast Values for Stored Energy

To solve the above problem and visually analyze the distribution of stored energy, band contrast (BC) values for every point in the testing region were collected from EBSD to estimate the distribution of stored energy at a micro-scale [11], as shown in Figure 6. Precisely, the BC value can reflect the extent to which different regions deformed upon rolling by detecting the grey levels corresponding to the maximum and minimum in the Hough transform procedure [24–26].

The stored energy S_i is proportional to the pattern quality index H_i as shown in the following relation [24]:

$$S_i \propto H_i = 10 \times \left[1 - \frac{Q_i(g_i) - Q_{min}}{Q_{max} - Q_{min}}\right] \quad (4)$$

S_i is stored energy for orientation 'i', H_i is the pattern index, Q_i (g_i) is the pattern quality for block 'i', and Q_{min} and Q_{max} are the minimum and maximum pattern qualities of the aggregate, respectively. Furthermore, based on such measurements, the distribution of stored energy in local areas of the surface was estimated. Thus, all surfaces were subdivided into 20 blocks (horizontal direction), as shown in Figure 5a, b. The stored energy value for each block was estimated and connected into lines in Figure 6c, d. Energy values fluctuated greatly through the thickness of the testing region in all three surfaces before and after annealing. More accurately, the values were large for {111} orientations or those closer to {111} due to the large dislocation density in {111} grains. In addition, the fluctuation degrees of energy values of the TD plane were much greater than those of the RD and ND planes in both deformed and annealed states.

Essentially, the annealing process is the rearrangement and annihilation of dislocations, which causes a decrease in dislocation density. So, are all regions equally degraded? Obviously not. This reduction in dislocation density is related to the dislocation distribution. Regions with high dislocation density are more likely to rearrange and form

new substructures, while regions with low dislocation density show the characteristics of slow kinetics.

Furthermore, not all dislocations rearrange. The dislocation movement is a thermal activation process, and the thermal activation temperatures of different dislocations are not the same. Simply put, at a temperature of 1073 K, only dislocation types that can be activated at temperatures below 1073 K can be activated [23]. Therefore, the process is affected by temperature, dislocation density, and type coupling.

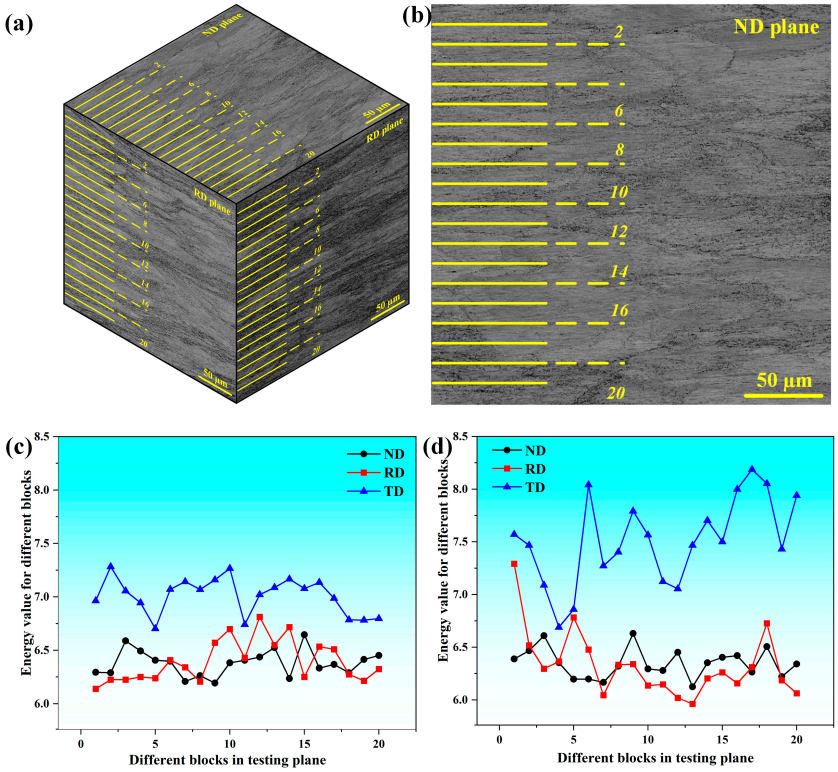

Figure 6. The BC map for different surfaces and the corresponding estimated stored energy. (**a**) Reconstructed orientation imaging maps (OIMs) of surfaces in three directions of the annealed sample, (**b**) the divided testing regions, (**c**) the energy evaluated for the deformed specimen, and (**d**) the energy evaluated for the annealed sample.

The difference in the stored energy distribution of different planes results from different dislocation densities, and dislocations are introduced via activations of slip systems in different grains. During rolling deformation, grains in the ND surface made contact with the roller. Next, they were compressed along the ND direction and extended along the RD direction, and evolved into 'pancake' shapes. As shown in Figure 7, the morphology of grains in the ND surface is related to the rolling direction, as marked by the green arrow. As a processing technique, rolling imposes a shear force (the force resulting from the downward pressure and forward friction) on the sheet plates, leading to the rearrangement of deformed grains along the shear direction, as shown in the TD plane in Figure 7. Grains experienced different degrees of splitting along the RD direction upon rolling; therefore, the microstructure of the RD surface was mainly composed of the ends or the cross-sections of the splitting grains, which were close to equiaxial shapes, as shown in the RD surface in Figure 7. From this point of view, the distribution of stored energy, which is mainly related to the boundaries of splitting grains, was homogeneous in the RD plane.

It should be emphasized that the trend in which the stored energy distribution of the RD surface was more homogeneous than that of the TD surface was consistent upon clock rolling. Thus, the fluctuation degree was not larger in the RD plane, as it was in the TD plane, as shown in Figure 6c. For the ND plane, using the same sized testing region as for

the TD and RD surfaces, only several 'pancake' grains were captured in the testing region; therefore, the distribution of stored energy was homogeneous in the testing region.

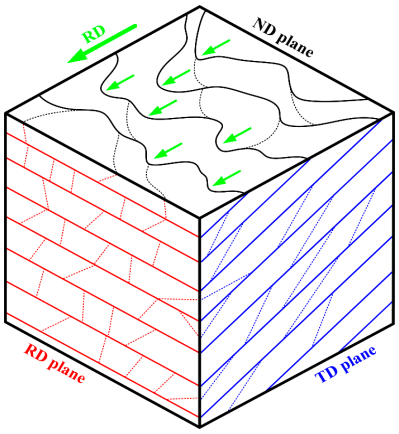

Figure 7. Schematic diagram of deformation microstructures in different surfaces upon rolling.

For the TD surface, as interpreted using XLPA, there was a large difference in stored energy between {111} and {100} orientations. Additionally, the alternate arranged {111} and {100} grains also played a positive role in the large fluctuation in the TD surface. Annealing of the TD surface resulted in a significant decrease in dislocation density, as shown in XLPA. Still, the decrease degrees were different for {111} and {100} grains due to their different recovery kinetics. From this point of view, as shown in Figure 8, an increased deformation degree or dislocation density led to distinct changes in substructures during consequent heating. Arrows in Figure 8b,d indicates the position of {100} orientations. There were almost no visible grain boundaries in annealed {100} grains, while boundaries were piled up everywhere in {111} grains, leading to significant fluctuation in the TD surface shown in Figure 8d.

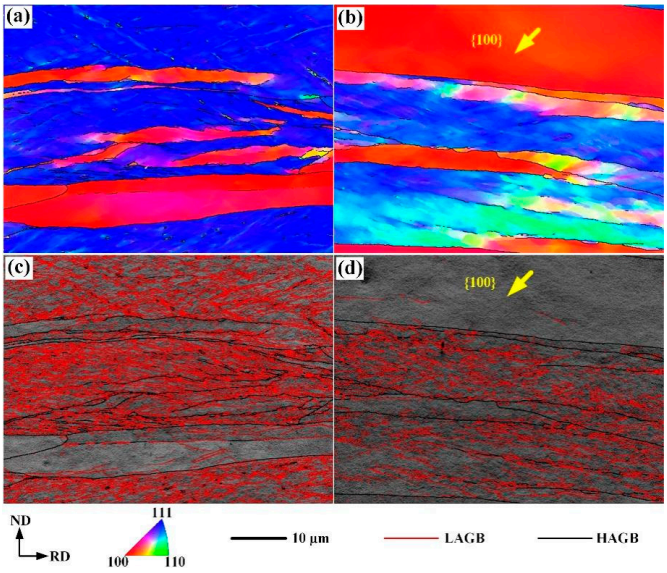

Figure 8. OIMs and corresponding grain boundary maps of deformed and annealed states, respectively, for TD surface. (**a**) OIM of deformed state; (**b**) OIM of annealed state; (**c**) grain boundary map of deformed state; and (**d**) grain boundary map of annealed state. LAGB, low angle grain boundary (2–10°); HAGB, high angle grain boundary (>10°).

5. Conclusions

In this paper, the microstructures of different surfaces of tantalum under deformed and annealed regimes were discussed, and the stored energy evolution was characterized and estimated by XLPA and BC values at macro and micro scales. The main findings are as follows:

(1) Microstructures, mainly composed of banded grains, were similar in TD and RD surfaces of deformed Ta due to the exchange of RD and TD surfaces along the changing rolling directions.

(2) There was a large difference in stored energy between deformed {111} and {100} grains. Annealing led to a significant decrease (about 64%) in {111} grains due to their large dislocation density in a deformed state.

(3) The fluctuation degree of stored energy on TD, RD, and ND surfaces was different. The degree of the TD surface was much larger than those of the RD and ND surfaces in the deformed and annealed regimes, which was mainly due to the alternating arrangement of {111} and {100} grains and their different recovery kinetics upon heating.

(4) When annealed at 1073 K, the dislocation density of {111} grains of tantalum was much lower than that of {100} grains. The degree of recovery was related to temperature, dislocation density, and dislocation type.

Author Contributions: Formal analysis, Y.Z. and Y.L.; funding acquisition, Y.Z. and Y.L.; methodology, Y.Z. and Y.L.; project administration, Y.Z.; writing—original draft, Y.Z. and Y.L.; writing—review and editing, Y.Z., Q.Z. and S.Y.; visualization, Y.L., Q.Z. and S.Y.; data curation, Q.Z. and S.Y. All authors have read and agreed to the published version of the manuscript.

Funding: This study was funded by the National Natural Science Foundation of China, grant number 52173297; the Key Research Project Plan for Higher Education Institutions in Henan Province, grant number 24ZX006; and Key R&D and promotion projects in Henan Province, grant number 222102230046.

Data Availability Statement: The raw/processed data required to reproduce these findings cannot be shared at this time as the data also forms part of an ongoing study.

Acknowledgments: Thanks to Chao Deng (Chongqing University) for the high-quality EBSD characterization, and to Shiyuan Zhou and Haoyan Tan for the enlightening discussion on dislocation and mechanical analysis.

Conflicts of Interest: The authors declare that they have no known competing financial interests or personal relationships that could have appeared to influence the work reported in this paper.

References

1. Cardonne, S.M.; Michaluk, P.K.C.A.; Schwartz, H.D. Tantalum and its alloys. *Int. J. Refract. Met. Hard Mater.* **1995**, *13*, 187–194. [CrossRef]
2. Michaluk, C.A. Correlating discrete orientation and grain size to the sputter deposition properties of tantalum. *J. Electron. Mater.* **2002**, *31*, 2–9. [CrossRef]
3. Robinson, M.T.; Southern, A.L. Sputtering experiments with 1- to 5- keV Ar + ions. III. monocrystal targets of the hexagonal metals Mg, Zn, Zr, and Cd. *J. Appl. Phys.* **1968**, *39*, 3463–3475. [CrossRef]
4. Robinson, M.T.; Southern, A.L. Sputtering experiments with 1- to 5- keV Ar + ions. II. monocrystalline targets of Al, Cu, and Au. *J. Appl. Phys.* **1967**, *38*, 2969–2973. [CrossRef]
5. Albou, A.; Raveendra, S.; Karajagikar, P.; Samajdar, I.; Maurice, C.; Driver, J.H. Direct correlation of deformation microstructures and cube recrystallization nucleation in aluminium. *Scr. Mater.* **2010**, *62*, 469–472. [CrossRef]
6. Mohamed, G.; Bacroix, B. Role of stored energy in static recrystallization of cold rolled copper single and multicrystals. *Acta Mater.* **2000**, *48*, 3295–3302. [CrossRef]
7. Zhang, Y.; Wang, J.T.; Cheng, C.; Liu, J. Stored energy and recrystallization temperature in high purity copper after equal channel angular pressing. *J. Mater. Sci.* **2008**, *43*, 7326–7330. [CrossRef]
8. Xia, J.Y.; Chai, L.J.; Wu, H.; Zhi, Y.; Gou, Y.N.; Huang, W.J.; Guo, N. EBSD study of microstructural and textural changes of hot-rolled Ti-6Al-4V sheet after annealing at 800 °C. *Acta Metall. Sin.* **2018**, *31*, 1215–1223. [CrossRef]
9. Zhao, Y.Q.; Chen, H.M.; Zhang, J.; Ma, R.; Liu, Y.D.; Wang, Y.N.; Wang, L.; Zhang, Q.; Li, W.G. Influences of asymmetric reduction rolling on the microstructure and mechanical properties of AZ91. *Acta Metall. Sin.* **2018**, *31*, 673–680. [CrossRef]

10. Liu, Y.H.; Liu, S.F.; Zhu, J.L.; Deng, C.; Fan, H.Y.; Cao, L.F.; Liu, Q. Strain path dependence of microstructure and annealing behavior in high purity tantalum. *Mater. Sci. Eng. A* **2017**, *707*, 518–530. [CrossRef]
11. Deng, C.; Liu, S.F.; Fan, H.Y.; Hao, X.B.; Ji, J.L.; Zhang, Z.Q.; Liu, Q. Elimination of elongated bands by clock rolling in high-purity tantalum. *Metall. Mater. Trans. A* **2015**, *46*, 5477–5481. [CrossRef]
12. Liu, Y.; Liu, S.; Deng, C.; Fan, H.; Yuan, X.; Liu, Q. Inhomogeneous deformation of {111}<uvw> grain in cold rolled tantalum. *J. Mater. Sci. Technol.* **2018**, *34*, 2178–2182.
13. Deng, C.; Liu, S.F.; Hao, X.B.; Ji, J.L.; Zhang, Z.Q.; Liu, Q. Orientation dependence of stored energy release and microstructure evolution in cold rolled tantalum. *Int. J. Refract. Met. Hard Mater.* **2014**, *46*, 24–29. [CrossRef]
14. Hupalo, M.F.; Sandim, H.R.Z. The annealing behavior of oligocrystalline tantalum deformed by cold swaging. *Mater. Sci. Eng. A* **2001**, *138*, 216–223. [CrossRef]
15. Kondo, S.; Mitsuma, T.; Shibata, N.; Ikuhara, Y. Direct observation of individual dislocation interaction processes with grain boundaries. *Sci. Adv.* **2016**, *2*, 1501926. [CrossRef]
16. Tanaka, Y.; Masumura, T.; Tsuchiyama, T.; Takaki, S. Effect of dislocation distribution on the yield stress in ferritic steel under identical dislocation density conditions. *Scr. Mater.* **2020**, *177*, 176–180. [CrossRef]
17. Zuiko, I.; Kaibyshev, R. Deformation structures and strengthening mechanisms in an Al-Cu alloy subjected to extensive cold rolling. *Mater. Sci. Eng. A* **2017**, *702*, 53–64. [CrossRef]
18. Li, Z.; He, B.; Guo, Q. Strengthening and hardening mechanisms of additively manufactured stainless steels: The role of cell sizes. *Scr. Mater.* **2020**, *177*, 17–21. [CrossRef]
19. Rajmohan, N.; Hayakawa, Y.; Szpunar, J.A.; Root, J.H. Neutron diffraction method for stored energy measurement in interstitial free steel. *Acta Mater.* **1997**, *45*, 2485–2494. [CrossRef]
20. Borbély, A.; Driver, J.H.; Ungár, T. An X-ray method for the determination of stored energies in texture components of deformed metals-application to cold worked ultra high purity iron. *Acta Mater.* **2000**, *48*, 2005–2016. [CrossRef]
21. Ikehata, H.; Nagasako, N.; Kuramoto, S.; Saito, T. Designing new structural materials using density functional theory: The example of gum metal. *MRS Bull.* **2011**, *31*, 688–692. [CrossRef]
22. Ruestes, C.J.; Stukowski, A.; Tang, Y.; Tramontina, D.R.; Erhart, P.; Remington, B.A.; Urbassek, H.M.; Meyers, M.A.; Bringa, E.M. Atomistic simulation of tantalum nanoindentation: Effects of indenter diameter, penetration velocity, and interatomic potentials on defect mechanisms and evolution. *Mater. Sci. Eng. A* **2014**, *613*, 390–403. [CrossRef]
23. Rez-Prado, M.T.P.; Hines, J.A.; Vecchio, K.S. Microstructural evolution in adiabatic shear bands in Ta and Ta-W alloys. *Acta Mater.* **2001**, *49*, 2905–2917. [CrossRef]
24. Choi, S.H.; Jin, Y.S. Evaluation of stored energy in cold-rolled steels from EBSD data. *Mater. Sci. Eng. A* **2004**, *371*, 149–159. [CrossRef]
25. Oyarzábal, M.; Martínez-de-Guerenu, A.; Gutiérrez, I. Effect of stored energy and recovery on the overall recrystallization kinetics of a cold rolled low carbon steel. *Mater. Sci. Eng. A* **2008**, *485*, 200–209. [CrossRef]
26. Wilkinson, A.J.; Dingley, D.J. Quantitative deformation studies using electron back scatter patterns. *Acta Metall. Mater.* **1991**, *39*, 3047–3055. [CrossRef]